J Appl Electrochem (2011) 41:397–403
DOI 10.1007/s10800-010-0249-9

ORIGINAL PAPER

Electrochromism in composite WO_3–Nb_2O_5 thin films synthesized by spray pyrolysis technique

S. H. Mujawar · A. I. Inamdar · C. A. Betty · R. Cerc Korošec · P. S. Patil

Received: 9 March 2010 / Accepted: 21 November 2010 / Published online: 8 December 2010

Abstract Composite WO_3–Nb_2O_5 thin films were deposited on the glass and fluorine-doped tin oxide (FTO)-coated glass substrates using simple and inexpensive spray pyrolysis technique. The process parameters, like nozzle-to-substrate distance, spray rate, concentration of sprayed solution, etc., were optimized to good quality films. The films were characterized for the structural, morphological, optical, and electrochromic properties. Structural and morphological characterizations of the films were carried out using scanning electron microscopy and X-ray diffraction techniques. Electrochemical properties of the Composite WO_3–Nb2O_5 thin films were further studied using cyclic-voltammetry, chronoamperometry, chronocoulometry, and electrochemical Impedance spectroscopy.

Keywords Composite WO_3–Nb_2O_5 thin films · Spray pyrolysis technique · Scanning electron microscopy (SEM) · X-ray diffraction (XRD)

S. H. Mujawar · A. I. Inamdar · P. S. Patil (✉)
Thin Film Materials Laboratory, Department of Physics, Shivaji University, Kolhapur 416 004, India
e-mail: psp_phy@unishivaji.ac.in; patilps_2000@yahoo.com

C. A. Betty
Chemistry Division, Bhabha Atomic Research Centre, Bombay, India

R. Cerc Korošec
Faculty of Chemistry and Chemical Technology, University of Ljubljana, Aškerčeva 5, 1000 Ljubljana, Slovenia

1 Introduction

The materials having ion intercalation and de-intercalation capability are emerging as electrodes for batteries, fuel cells, and electrochromic (EC) devices. EC materials are able to exhibit persistent and reversible changes in their optical properties under the application of voltage. Several efforts are being made to enhance optical modulation, coloration efficiency (CE), and chemical stability of the materials. The EC behavior is described in terms of simultaneous injection or extraction of electrons and ions, depending on polarity of the applied voltage. The EC material should have a structure that is permeable enough for easy intercalation and de-intercalation of ions. The intercalated ions can diffuse and reside in the spaces between the MeO_6 octahedra. However, at least for the framework structure, these spaces may not be large enough to yield reasonable intercalation/de-intercalation rates, and therefore the material must have fine-grained or amorphous structure. Thus, major impetus on developing good quality EC material has been on tailoring the structure to improve electronic conductivity and ionic diffusivity.

We have earlier reported synthesis and characterization of EC Nb_2O_5 thin films by simple and inexpensive spray pyrolysis technique [1]. Also from the post-annealing treatment [2], it is observed that the EC performance degrades after the annealing treatment, i.e., CE decreases from 13 to 10 $cm^2\ C^{-1}$ and EC reversibility decreases from 85 to 71%. The observed degradation in the EC performance is attributed to the decrease in the grain boundary area due to the improvement in the crystallinity of Nb_2O_5 thin films, which limits the diffusivity of ions into the film.

Binary combinations of oxides have been investigated to improve the EC properties of different oxides. Possible beneficiary effects on the host EC material are increased

CE, improved durability, color neutrality, a larger switching potential range, or faster reaction kinetics. Both Granqvist and Monk [3, 4] recently reviewed mixed metal oxides and presented useful summary. An improvement in reversibility was reported by adding TiO_2 in WO_3 [5]. WO_3 films doped with MoO_3 exhibits profound electrochromism [6]. Among a broad range of mixed elements (Ni, Cr, Ti, Nb, etc.), films containing less than 20% V were presented as being most promising for its color neutrality in its reduced state; similar results are reported in literature [7–9]. Some results pertaining to Sn, Zr, Li, Mo, and TiO_2-doped Nb_2O_5 were reported [10–12]. Recently, improvements in the EC properties of sol–gel prepared TiO_2 and WO_3-doped Nb_2O_5 thin films have been reported [13, 14].

In this study efforts have been made to preserve the amorphous nature of Nb_2O_5 films, by preparing their composite with WO_3. The EC properties of the WO_3–Nb_2O_5 thin films are studied. The results are discussed, and plausible mechanism for the improvement in EC performance is put forward.

2 Experimental

2.1 Preparation of solutions

The composite thin films of WO_3–Nb_2O_5 were deposited by spray pyrolysis technique. The preparation method for the starting solution of niobium is discussed in detailed in Ref. [1]. Precursor solution of tungsten was prepared by dissolving WO_3 powder in the ammonia at 80 °C and diluted by deionized water to the required concentration. The equimolar (0.005 M) solutions of Nb:W were further added in proper proportions to achieve 10, 20, 30, and 40% mixing of WO_3 in Nb_2O_5. The solution was homogeneous and transparent over entire composition range. The final solution (50 ml) was pneumatically pulverized on the hot glass and fluorine-doped tin oxide conducting hot glass substrates maintained at 450 °C. The 10, 20, 30, and 40% WO_3-mixed Nb_2O_5 samples are denoted as NW_{10}, NW_{20}, NW_{30}, and NW_{40}, respectively. Film thickness was measured using XP-1 surface profiler and was found to vary between 520 and 530 nm.

2.2 Characterizations

Thermogravimetric measurements were performed on a Mettler Toledo TGA/SDTA 851^e instrument from 25 to 650 °C. The film deposited on to platinum (2.5 cm^2) substrate was placed into sample holder. Heating rate of 5 K min^{-1} was used for dynamic measurement. The furnace was purged with air at 100 mL min^{-1} flow rate. Film thickness was measured using a gravimetric method. The structural and morphological characterizations were carried out using a Philips PW 3710 X-ray diffractometer with CuKα radiation (wavelength 1.5432 Å), and scanning electron microscopy (SEM) JEOL JSM 6360, respectively. The optical characterization was carried out using UV–Vis Systronic spectrophotometer in the wavelength range from 350 to 850 nm. Electrochemical impedance measurements were carried out at room temperature by Frequency Response Analyzer attached with potentiostat PGSTAT AUTOLAB 20 (Echo Chemie Netherlands) at 0.7 V bias voltages using a small ac signal of 10 mV peak to peak in the frequency range 0.1 Hz–700 kHz. Electrochemical measurements were performed using EG and G make VersaStat-II model, controlled by electrochemistry software M270.

3 Results and discussion

3.1 Thermo-gravimetric analysis (TGA)

To study the decomposition behavior of the precursor material on the basis of the measured weight loss and hence to optimize the film formation temperature, TGA of the composite film over a platinum substrate of area 2.5 cm^2 was carried out. Figure 1 shows the TGA plot for the composite WO_3–Nb_2O_5 film with 1:1 composition, deposited at 200 °C under ambient atmosphere. The weight loss due to decomposition of composite was observed in two steps: Step I—from room temperature to 150 °C, removal of physisorbed and chemisorbed water; and Step II—300–450 °C, removal of tartaric acid and ammonia complexes. After 500 °C, weight remains constant up to 650 °C. Hence, we inveterate composite WO_3–Nb_2O_5 film formation is at about 450 °C.

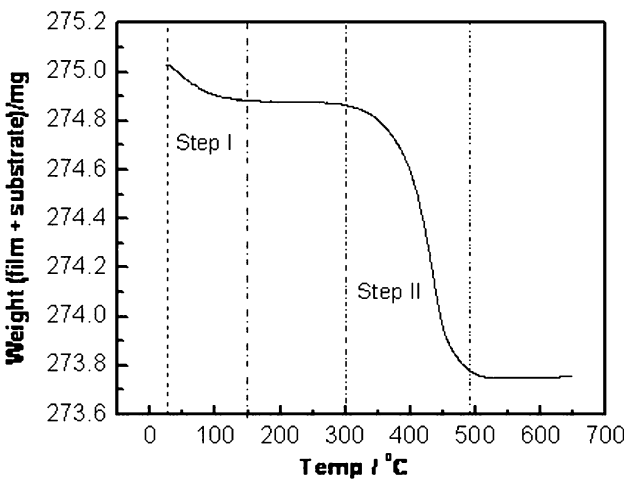

Fig. 1 Dynamic thermo-gravimetric plot recorded for WO_3–Nb_2O_5 thin film deposited at 200 °C under ambient atmosphere

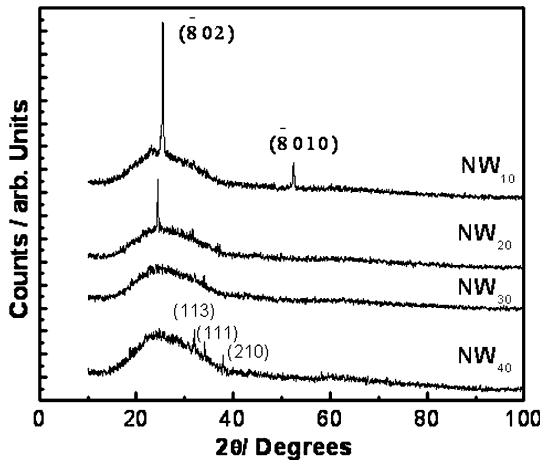

Fig. 2 X-ray diffraction spectra recorded for NW_{10}, NW_{20}, NW_{30}, and NW_{40} sample

3.2 X-ray diffraction (XRD)

Figure 2 compares the XRD spectra for NW_{10}, NW_{20}, NW_{30}, and NW_{40} samples. It is observed that with increase in WO_3 content in the composite intensity of X-ray peaks along $(\bar{8}02)$ and $(\bar{8}010)$ corresponding to monoclinic phase of Nb_2O_5 decrease, and the sample NW_{30} do not exhibit any signature of crystallinity, broad hump centered at 24 is characteristic of amorphous glass substrate. Sample NW_{40} exhibits dominant growth of WO_3 phase over the Nb_2O_5 host material, with emerging reflections along (113), (111), and (210) planes. This is the onset of WO_3 crystallization and Nb_2O_5 becomes amorphous. It is clear that the addition of the WO_3 to Nb_2O_5 impedes the growth of Nb_2O_5 and leads to formation of an amorphous structure. The growth mechanism is not yet fully understood and warrants further study.

3.3 Scanning electron microscopy (SEM)

Figure 3a, b, c, d shows scanning electron micrographs for the NW_{10}, NW_{20}, NW_{30}, and NW_{40} samples, respectively. Sample NW_{10} exhibits coral reef-like structure containing 2 μm floral feature to about 7-μm-long reefs. Upon raising WO_3 percentage (NW_{20}), coral reef-like structure dominates, and spreads uniformly over the surface. The surface morphology of NW_{30} sample is almost featureless, with blurred floral-like imprints. A unique snowflake-like morphology is clearly seen in NW_{40} sample.

3.4 Electrochemical characterizations

For the electrochemical characterization, the standard three-electrode electrochemical cell of following configuration was used:

$$\mathrm{Glass/FTO/WO_3-Nb_2O_5/0.5\,M\ H_2SO_4/C/SCE}$$

where WO_3–Nb_2O_5 thin film acts as a working electrode, and H_2SO_4 is an H^+ ion source electrolyte. A saturated Calomel electrode (SCE) was used as a reference electrode

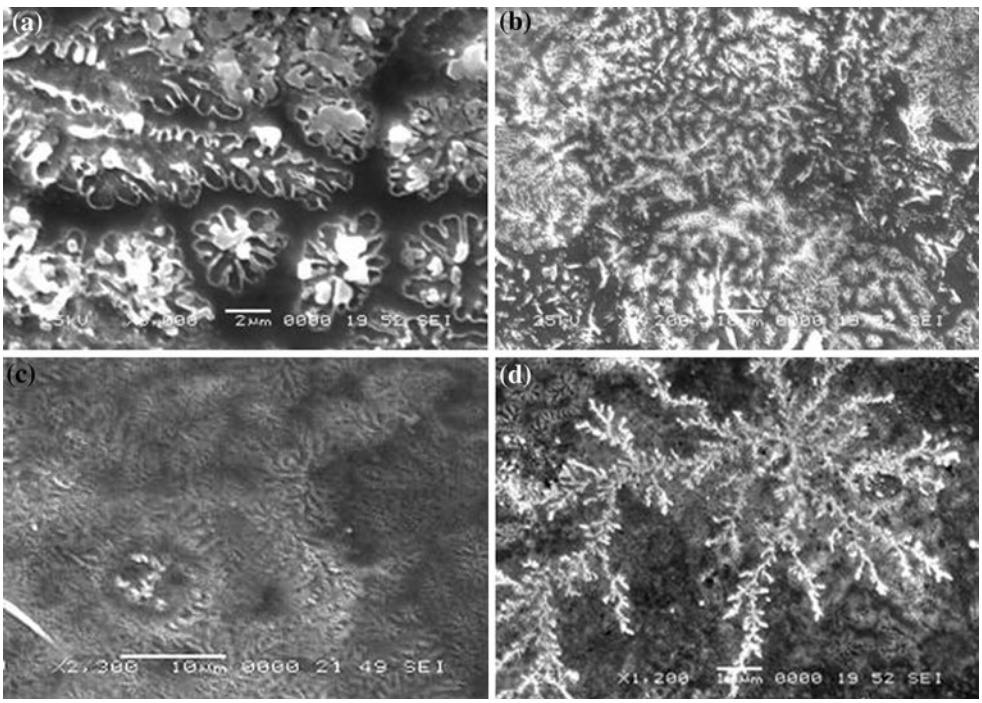

Fig. 3 **a–d** SEM micrographs for sample NW_{10}, NW_{20}, NW_{30}, and NW_{40}, respectively

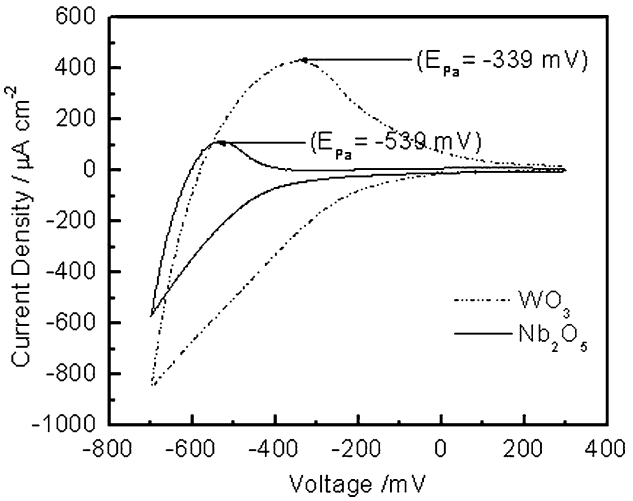

Fig. 4 The cyclic voltammogram recorded for the pristine Nb_2O_5 and WO_3 samples

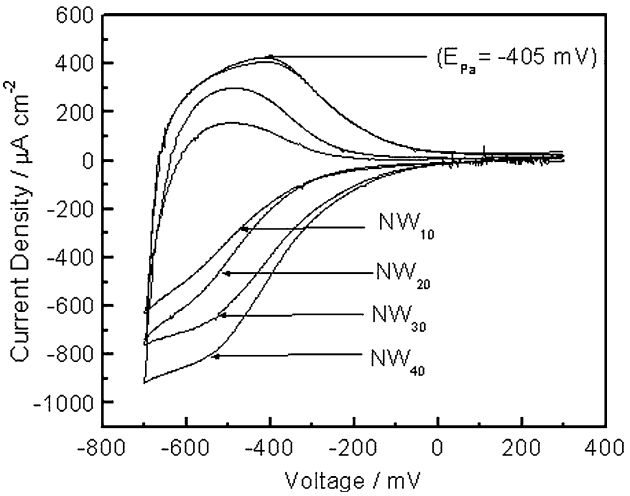

Fig. 5 The cyclic voltammograms recorded for NW_{10}, NW_{20}, NW_{30}, and NW_{40} samples

to which all measured voltages were referred; C is platinum wire (helical), which acts as counter electrode.

3.4.1 Cyclic voltammetry

Figure 4 shows electrochemical cyclic voltammograms (CVs) for the pristine Nb_2O_5 and WO_3 samples in the potential range +300 to −700 mV (SCE), at 100 mV s^{-1}. For the pristine Nb_2O_5 and WO_3 samples, the anodic peak potential is located at −539 and −339 mV, respectively.

Figure 5 shows CVs recorded for the NW_{10}. NW_{20}, NW_{30}, and NW_{40} sample. The appearance of a cathodic and the second anodic peak suggest the occurence of new redox process as a consequence of the dopage, which entails formation of composite structure in the thin film form. Also, the observed shape of CV suggests that it is because of the composite structure of both Nb_2O5 and WO_3. From Fig. 5, it is observed that threshold voltage (E_Γ) shifts toward positive potential (from −380 to −205 mV) with increase in percentage of WO_3, indicating that doped structures are more favorable for easy insertion of H^+ ions. A shift in anodic peak potential (E_{pa}) from −512 to −405 mV indicates that the energy required to extract the intercalated H^+ ions from the film decreases with increase in percentage of WO_3. This suggests that the amorphous structure promotes an easy way to diffusion of H^+ ions. With the increase in WO_3 percentage, both IPc and IPa increase linearly with bulging in the voltammograms showing higher charge insertion density than that of for pure WO_3 and Nb_2O_5 (Fig 4) over the same scanning potential range, indicating faster rate of kinetics. All the samples exhibit deep grayish-blue color upon ion intercalation and retain transparent state upon ion de-intercalation. The increase in the area of voltammograms and overlapping of anodic peaks for samples NW_{30} and NW_{40} shows saturation in oxidation reaction, and hence limits EC reversibility. The diffusion constant for the H^+ ions (D_{H+}) is calculated using the relation (1):

$$D^{1/2} = \frac{I_{pc}}{2.72 \times 10^5 \times n^{3/2} \times C_o \times A \times v^{1/2}} \quad (1)$$

where Ipc = cathodic peak potential, v = scan rate (mV s^{-1}), n = number of electrons, C_o = electrolyte concentration (0.5 M), and A = Area of film.

The calculated values of D_{H+} are mentioned in the Table 1. With increase in WO_3 percentage, D_{H+} increases from 1.4×10^{-7} to 2.2×10^{-7} cm^2 s^{-1} which clearly entails that the composite structure favors ion intercalation/de-intercalation in preference to the pristine structure. This pronounced difference stems from the amorphous nature of the sample. Also, the samples exhibit higher electrochemical stability even after 1000 cycles.

3.4.2 Chronoamperometry (CA)

The response time for an EC material is defined as the time required for the intercalation/de-intercalation current to stabilize at its lowest value. The coloration time (t_c) and bleaching time (t_b) were calculated from the current

Table 1 Various parameters obtained from cyclic voltammetry and chronoamerometric studies of WO_3–Nb_2O_5 thin films

Sample Id	Response time		Diffusion constant (cm^2 s^{-1})
	t_c (s)	t_b (s)	
NW_{10}	3.2	1.3	1.4×10^{-7}
NW_{20}	3.8	1.8	1.8×10^{-7}
NW_{30}	4.3	2.2	2.0×10^{-7}
NW_{40}	5.1	2.6	2.2×10^{-7}

time transients recorded using chronoamperometry (CA) technique. During the experiment, the voltage was stepped from its rest potential of 0.0 to −0.5 V for 10 s (Coloration) and then reversed to +0.5 V for next 10 s (bleaching). It is observed that with increase in percentage of WO_3 coloration and bleaching, kinetics becomes easier and faster. The response time for all the samples is calculated from these CA plots and is reported in Table 1.

3.4.3 Chronocoulometry (CC)

To study H + ion intercalation, de-intercalation processes with respect to time, chronocoulometry was carried out at potential steps of ∓ O.5 V (versus SCE), for a step of 10 s. Amount of charge intercalated (Q_i), amount of charge de-intercalated (Q_{di}), and hence residual charge (Q_i–Q_{di}) has been calculated. The calculated values of (Q_i), (Q_{di}) and (Q_i–Q_{di}) are given in Table 2. The EC reversibility of the Nb_2O_5 film is calculated using relation (2)

$$\text{reversibility} = \frac{\text{Qdi}}{\text{Qi}} \tag{2}$$

It is observed that Qi and Qdi both increase whereas (Qi–Qdi) decreases, with increase in WO_3 percentage and hence EC reversibility increases from 88 to 90%. For pure Nb_2O_5 thin film, prepared by spray pyrolysis technique, it was 85%. Hence, it is concluded that amorphous structure is favorable for EC mechanism.

3.4.4 Iono-optical studies

To color (reduce) and bleach (oxidize) the composite thin films, the potential step of ∓ O.5 V (versus SCE), for constant time (10 s) is applied. The transmittance spectra for all the four samples in their colored and bleached states were recorded in the wavelength range from 350 to 850 nm, at the room temperature. Figure 6 shows comparative transmittance spectra recorded for NW_{10} and NW_{40} samples in its colored (C) and bleached (B) states. The optical absorption by the thin layer is described by the dimensionless quantity (αt), which is called as optical density (OD). The change in optical density (ΔOD) is calculated using the relation (3):

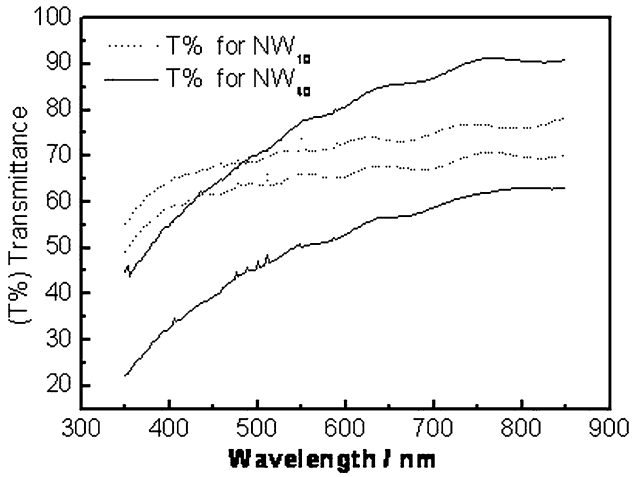

Fig. 6 Transmission spectra for NW_{10} and NW_{40} sample in its colored (C) and Bleached state (B)

$$\Delta\text{OD} = \log\left(\frac{T_b}{T_c}\right) \tag{3}$$

where T_b and T_c are the transmittances of the Nb_2O_5 film in its colored and bleached states, respectively.

The coloration efficiency (CE) is defined as the change in optical density (ΔOD) per unit inserted charge and is calculated using the relation (4):

$$\text{CE} = \frac{\Delta\text{OD}}{\Delta Q} \tag{4}$$

where ΔQ is the amount of charge intercalated in the sample to cause change in optical density (ΔOD). Calculated values of reversibility and CE with respect to WO_3 composition are given in Table 2. It has been observed that with increase in percentage transmittance, modulation (ΔT) increases from 6 to 30%, which improves OD, and, hence, CE increases from 17 to 26 $cm^2\ C^{-1}$.

3.5 Kroger and Vink equation

The observed overall improvement in the EC parameters can be explained with the help of Kroger and Vink notations. Following equation can be written in the present case:

Table 2 Various electrochromic parameters calculated from electrochemical and iono-optical studies of WO_3–Nb_2O_5 thin films

Sample ID	T_b (%)	T_c (%)	ΔOD	Qi (mC cm^{-2})	Qdi (mC cm^{-2})	Reversibility = (Qdi/Qi)	CE ($cm^2\ C^{-1}$)
NW_{10}	73	67	0.03	1.7	1.5	88	17
NW_{20}	74	64	0.06	3.0	2.7	89	20
NW_{30}	80	60	0.12	4.7	4.1	90	25
NW_{40}	85	55	0.18	6.9	6.2	90	26

$$2WO_3 \xrightarrow{Nb_2O_5} 2W^{\bullet}_{Nb} + 5O^{\times}_{O} + O''_i$$

When two ions of Nb were replaced by two ions of W then to maintain the charge neutrality in the lattice, an oxygen ion is forced at the interstitial site. The oxygen ion forced at the interstitial site causes the disordering in the structure because of its larger ionic radii than those of Nb and W, and, hence, opens up more channels for the insertion of H^+ ions as well as improves the electronic conductivity of the material.

3.5.1 Electrochemical impedance spectroscopy (EIS)

The real and imaginary parts of the measured impedance are plotted in Fig. 7. The plots indicate that for sample NW_{10}, a third semicircle in the mid-frequency range appears. With increase in WO_3 percentage, the observed semicircle in the mid-frequency region disappears and also diffusion resistance decreases which clearly entails that, for crystalline samples, intergranular transport as well as the diffusion of ions through grain boundaries become more difficult. In contrast, amorphous structure leads the electrode properties toward ideal diffusion process. Impedance data have been fitted using an equivalent circuit as shown in the Fig. 8. The equivalent circuit fits the impedance data as clearly seen in the figure. In this circuit, R_s represents the contact and electrolyte resistance, Q_b, Q_g, and Q_i represent the bulk grain (intragrain), grain boundary, and intergrain capacitive contributions, respectively, which are frequency dependant and represented by constant phase elements (CPEs). W represents the impedance contribution due to the diffusion of ions through grain boundaries. R_b, R_g, and R_i represent the corresponding resistive contributions. Admittance Versus frequency plots, Fig. 9, also show that there is a decrease in conductivity in the mid-frequency region for sample NW_{10} whereas with respect to increase in percentage of WO_3, conductivity increases.

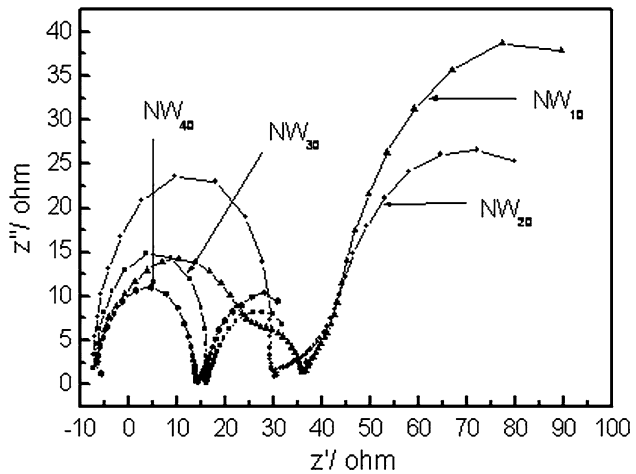

Fig. 7 Plot Z′ versus Z″ for NW_{10}, NW_{20}, NW_{30}, and NW_{40} sample

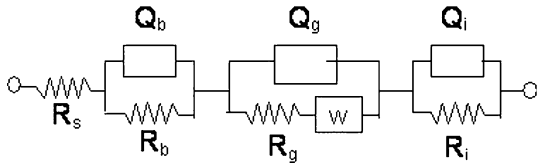

Fig. 8 Equivalent circuit

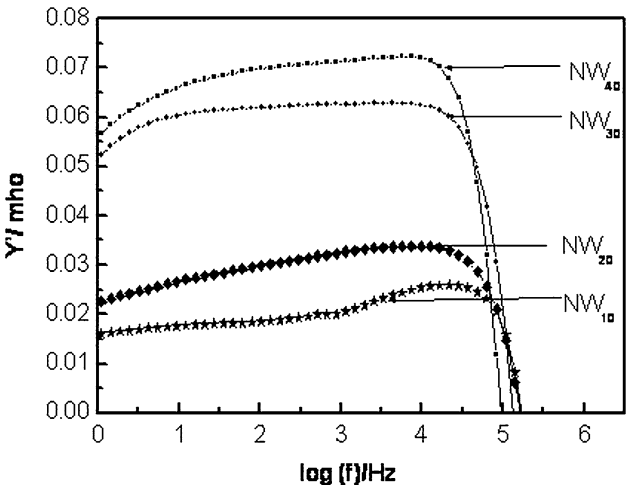

Fig. 9 Plot of Y′ versus log (*f*) for NW_{10}, NW_{20}, NW_{30}, and NW40 sample

4 Conclusions

Composite WO_3–Nb_2O_5 thin films were successfully prepared using simple and inexpensive spray pyrolysis technique. With increase in the percentage of tungsten oxide, the negative effect on the crystallization of composite WO_3–Nb_2O_5 thin film has been observed. Preservation of amorphous structure improves the EC properties of composite WO_3–Nb_2O_5, by offering more conducive channels for the intercalation–de-intercalation of H^+ ions in the thin films. Sample NW_{40} exhibits best EC properties, viz., $CE = 26\ cm^2\ C^{-1}$ and EC reversibility = 90%.

Acknowledgments Authors are very much thankful to the CSIR, New Delhi for the financial support extended through Senior Research Fellowship (SRF).

References

1. Mujawar SH, Inamdar AI, Patil SB, Patil PS (2006) Solid State Ionics 177:3333
2. Mujawar SH, Inamdar AI, Betty CA, Ganesan V, Patil PS (2007) Electrochim Acta 52:4899

3. Granqvist CG (1995) Handbook of inorganic electrochromic materials. Elsevier Publication, Amsterdam
4. Monk PMS, Mortimer RJ, Rosseinsky DR (1995) Electrochromism fundamental and applications. VCH, Weinheim
5. Hashimoto S, Matsuoka H (1991) J Electrochem Soc 138:2403
6. Pennisi A, Simone F, Lampert CM (1992) Sol Energy Mater Sol Cells 28:223
7. Rougier A, Blyr A, Quede A (2001) J Electrochem Soc 148(2):H7
8. Ozer N, Lampert CM (1999) Thin Solid Films 349:205
9. Richardson TJ, Von Rottkay K, Slack J, Michalak F, Rubin M (1998) Electrochem Soc Proc 98–26 158
10. Schmitt M, Aegerter MA (2001) Electrochim Acta 46:2105
11. Rosario AV, Pereira EC (2001) Electrochim Acta 46:1905
12. Costa ED, Avellaneda CO, Pawlicka A (2001) J Mater Sci 36:1407
13. Pehlivan E, Tepehan FZ, Tepehan GG (2005) Sol Energy Mater Sol Cells 87:317–322
14. Pehlivan E, Tepehan FZ, Tepehan GG (2003) Solid State Ionics 165:105–110